

Magnonic band-pass and band-stop filters with structurally modulated waveguides

Lai-He Feng(冯来和), Mang-Yuan Ma(马莽原), Zhi-Hua Liu(刘智华), Kai-Le Xie(解凯乐), and Fu-Sheng Ma(马付胜)

Citation: Chin. Phys. B, 2023, 32 (**6**): 067503. DOI: 10.1088/1674-1056/ac8afb
Journal homepage: http://cpb.iphy.ac.cn; http://iopscience.iop.org/cpb

What follows is a list of articles you may be interested in

Angle-dependent spin wave spectra of permalloy ring arrays

Shuxuan Wu(吴书旋), Zengtai Zhu(朱增泰), Yunxu Ma(马云旭), Jinwu Wei(魏晋武), Senfu Zhang(张森富), Jianbo Wang(王建波), and Qingfang Liu(刘青芳)

Chin. Phys. B, 2022, 31 (**11**): 117505. DOI: 10.1088/1674-1056/ac8af9

Experimental observation of interlayer perpendicular standing spin wave mode with low damping in skyrmion-hosting $[Pt/Co/Ta]_{10}$ multilayer

Zhen-Dong Chen(陈振东), Mei-Yang Ma(马眉扬), Sen-Fu Zhang(张森富), Mang-Yuan Ma(马莽原), Zi-Zhao Pan(潘咨兆), Xi-Xiang Zhang(张西祥), Xue-Zhong Ruan(阮学忠), Yong-Bing Xu(徐永兵), and Fu-Sheng Ma(马付胜)

Chin. Phys. B, 2022, 31 (**11**): 117501. DOI: 10.1088/1674-1056/ac7bf9

Interaction region of magnon-mediated spin torques and novel magnetic states

Zai-Dong Li(李再东), Qi-Qi Guo(郭奇奇), Yong Guo(郭永), Peng-Bin He(贺鹏斌), and Wu-Ming Liu(刘伍明)

Chin. Phys. B, 2021, 30 (**10**): 107506. DOI: 10.1088/1674-1056/ac04a8

Spin waves and transverse domain walls driven by spin waves: Role of damping

Zi-Xiang Zhao(赵梓翔), Peng-Bin He(贺鹏斌), Meng-Qiu Cai(蔡孟秋), Zai-Dong Li(李再东)

Chin. Phys. B, 2020, 29 (**7**): 077502. DOI: 10.1088/1674-1056/ab90e5

Voltage control of ferromagnetic resonance and spin waves

Xinger Zhao(赵星儿), Zhongqiang Hu(胡忠强), Qu Yang(杨曲), Bin Peng(彭斌), Ziyao Zhou(周子尧), Ming Liu(刘明)

Chin. Phys. B, 2018, 27 (**9**): 097505. DOI: 10.1088/1674-1056/27/9/097505

Magnonic band-pass and band-stop filters with structurally modulated waveguides

Lai-He Feng(冯来和), Mang-Yuan Ma(马莽原), Zhi-Hua Liu(刘智华), Kai-Le Xie(解凯乐), and Fu-Sheng Ma(马付胜)†

Jiangsu Key Laboratory of Opto-Electronic Technology, School of Physics and Technology, Nanjing Normal University, Nanjing 210046, *China*

(Received 17 May 2022; revised manuscript received 3 August 2022; accepted manuscript online 19 August 2022)

Magnonics is a fascinating and emerging field, which mainly studies processing information with spin waves. Magnonic devices with in-plane magnetization have recently been realized. Because of the isotropic propagation, magnonic devices based on perpendicular magnetization are attracting extensive interest. Here, we numerically demonstrate two magnonic filters with out-of-plane magnetization using micromagnetic simulations. The band-pass and the band-stop functions have been realized in two structurally modulated waveguides, respectively. The intensity of spin waves is manipulated when they arrive at the uniformly/non-uniformly magnetized modulators, which results in the variation of transmission coefficients. It is found that the proposed filters can work at multiple frequencies, which can be further adjusted by the external magnetic field. Our designed magnonic devices with Néel-type skyrmion could promote the development of spin wave computing using spin textures.

Keywords: spin waves, filter, micromagnetic simulation, skyrmion

PACS: 75.75.–c, 75.78.Cd, 85.70.–w **DOI:** 10.1088/1674-1056/ac8afb

1. Introduction

Breakthroughs in complementary metal–oxide–semiconductor (CMOS) technology are difficult to achieve because of the inherent physical limits caused by quantum effects and power loss caused by charge effects.[1,2] To solve these obstacles, researchers have proposed various alternative devices, including tunneling field-effect transistors,[3] graphene nanoribbon field-effect transistors,[4] magnonic devices,[5,6] etc. Magnonic devices use magnons,[7–9] the quanta of spin waves, to transfer information without any motion of real particles. Compared with conventional charge-based devices, magnonic devices have no Ohmic loss.[10] Furthermore, they can work in the frequency range from GHz to THz[11] and provide a variety of information encoding methods including amplitude encoding[12] and phase encoding.[13] These advantages make spin waves a superior alternative for processing information for low-energy computing devices[14,15] and provide a broader and brighter prospect for the development of information technology.[16]

In the last decade, a large number of magnonic data-processing devices[17–19] have been proposed and realized, for instance, transistors,[20] logic gates,[12,21,22] phase shifters,[23] directional couplers,[24] and majority gates.[25,26] These devices utilize the interference of magnons,[12] the non-anisotropy of spin waves,[22] and the width modulation of transmission waveguides[27] to perform their functions.

Up to now, magnonic devices have been used for complete Boolean computing[26] and non-Boolean logic computing.[28,29] They also show infinite possibilities in radio frequency applications[30] and neuromorphic computing[31,32] on the nanometer scale. So far, most studies have been carried out in in-plane magnetized systems. Because of the isotropic propagation, magnonic devices based on perpendicular magnetization are attracting extensive interest. Besides, perpendicular magnetization can overcome the superparamagnetic limit and obtain thermal stability. In addition, the presence of the Dzyaloshinsky–Moriya interaction (DMI)[33,34] would not only introduce the nonreciprocal propagation of spin waves but also result in the nucleation of spin textures such as domain walls[35] and skyrmions.[36]

In this work, we have numerically implemented amplitude-type filters based on a structurally modulated magnonic waveguide with perpendicular magnetization by micromagnetic simulations. It is found that the band-stop and the band-pass functions can be realized by manipulating the intensity of spin waves when they arrive at the uniformly/non-uniformly magnetized modulators, which results in the variation of transmission coefficients. In addition, we find that the proposed filters can work at multiple frequencies, which can be further adjusted by the external magnetic field.

2. Simulation method

MuMax^3 was used for the micromagnetic simulation.[37] It is a GPU-based open-source software that solves Landau–Lifshitz–Gilbert equations through the finite difference method. The simulated structures of the filters are shown in Fig. 1(a). The cell size was set to 1 nm × 1 nm × 1 nm and the magnetic parameters were derived from CoFeB:[38,39] saturation magnetization $M_s = 1.6 \times 10^6$ A/m, exchange constant $A = 16 \times 10^{-12}$ J/m, perpendicular magnetic anisotropy

†Corresponding author. E-mail: phymafs@njnu.edu.cn

© 2023 Chinese Physical Society and IOP Publishing Ltd

constant $K_u = 2 \times 10^6$ J/m^3, adapted DMI constant $D = 3.0$ mJ/m^2, and Gilbert damping parameter $\alpha = 0.001$. An absorption boundary condition is applied at the ends of the magnonic waveguide to avoid reflections of spin waves.

To excite spin waves ranging from 0 GHz to 100 GHz, a "Sinc" perturbation field h_x is applied in the orange region in Fig. 1(a): $h_x(t) = h\sin(2\pi f_{cut}t)/(2\pi f_{cut}t)$,[40] where $h = 10$ mT and $f_{cut} = 100$ GHz, while a sinusoidal perturbation field $h_x(t) = h\sin(2\pi ft)$ is applied to excite a spin wave with a specific frequency f. For each case, the perturbation field was applied continuously for 10 ns, during which the magnetization $m(x,y,z,t)$ was saved every 5 ps. To obtain the transmission of the spin-wave in the device, we selected four calculation regions within a range of 20 nm at the input-port as the writing-area and four regions at the output-port as the reading-area, shown as the blue and red regions in Fig. 1(a), respectively. The averaged magnetization $m(x,y,z,t)$ of the writing- and reading-areas was saved. Then, a Fourier transform was performed on the magnetization $m_x(t)$ to obtain amplitudes of the magnetization $m_x(f)$ of each region. Next, we averaged the amplitudes of the writing- and reading-areas as A_1 and A_2, respectively. Finally, the transmission coefficient T was calculated as the ratio of the spin-wave intensity at the writing- and the reading-areas, $T = A_2^2/A_1^2$.

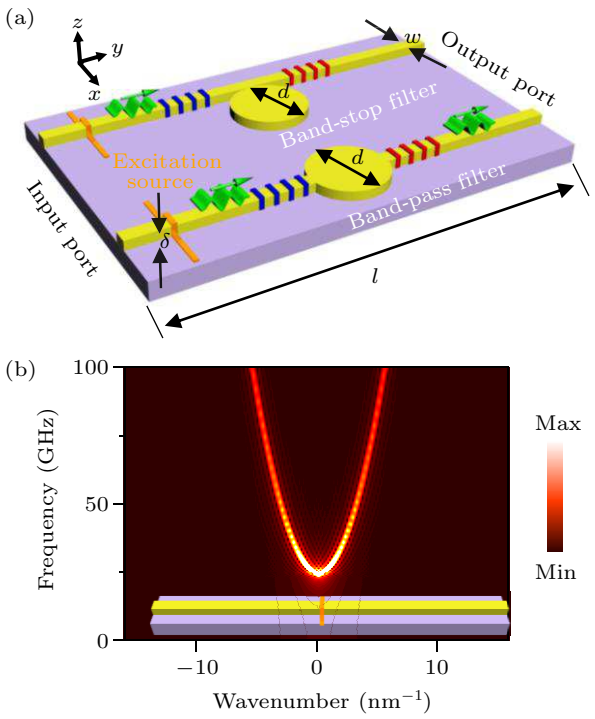


Fig. 1. (a) Schematics of magnonic filters: a band-stop filter (up) and a band-pass filter (down). The dimensions of the simulated filters are the length $l = 600$ nm, width $w = 10$ nm, thickness $\delta = 1$ nm, and diameter $d = 40$ nm. Green arrows represent the propagation of spin waves. Orange areas represent the positions of the excitation source. Blue and red areas represent the positions for calculating spin wave transmission. (b) Magnonic dispersion of the waveguide at $H_z = 0$ mT. Inset indicates the schematic of a waveguide with the same dimensions l, w, δ as in panel (a).

3. Results

In this work, we realized two kinds of magnonic filters: the band-pass filter and the band-stop filter, as shown in Fig. 1(a). The simulated filters are in the form of structurally modulated waveguides with dimensions as follows: length $l = 600$ nm, width $w = 10$ nm, and thickness $\delta = 1$ nm; the modulator was in the form of a circular disk with diameter $d = 40$ nm and thickness $\delta = 1$ nm. Figure 1(b) is the calculated dispersion diagram of spin waves propagating in the waveguide without the presence of a modulator under zero field. There is a frequency threshold about 25 GHz.

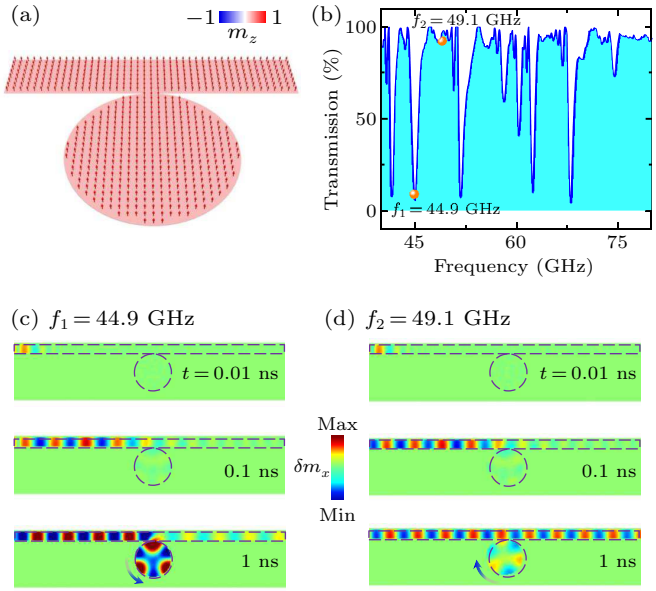


Fig. 2. (a) Magnetization of uniformly magnetized band-stop filter. (b) Calculated transmission of spin waves with different frequencies. Temporal snapshots of spin waves propagating in the filter at $t = 0.01$ ns, 0.1 ns, and 1 ns for (c) $f_1 = 44.9$ GHz and (d) $f_2 = 49.1$ GHz as marked in panel (b).

Firstly, we studied the transmission characteristics of spin waves in the band-stop filter shown in Fig. 1(a), in which there is a circular modulator tangent to the waveguide. Figure 2(a) schematically shows the magnetization of the band-stop filter, which is uniformly magnetized out-of-plane. Figure 2(b) shows the calculated transmission coefficients of spin waves at various frequencies from 40 GHz to 80 GHz under zero field $H_z = 0$ mT. It is found that spin waves can almost completely transmit from the input-port to the output-port at most frequencies, where their transmission coefficient can be as high as 90% or even more. However, spin waves with a few frequencies cannot go past the waveguide, with their transmission coefficient being as low as 10% or even less. Therefore, the magnonic model shown in Fig. 2(a) can realize the function of a band-stop filter, and it can even work at multiple frequencies. For the case of disks with spin texture, spin waves exhibit similar transmission characteristics. And only band-stop filters with simple magnetic structures are discussed here. To observe the intensity distribution of spin waves with

high and low transmission coefficients, we selected two typical frequencies: $f = 44.9$ GHz with low transmission $T = 9\%$; and $f = 49.1$ GHz with high transmission $T = 92\%$, as indicated by orange circles in Fig. 2(b). Figures 2(c) and 2(d) are the temporal snapshots of spin-wave propagation in the filter at time $t = 0.01$ ns, 0.1 ns, and 1.0 ns. By comparing Figs. 2(c) and 2(d), spin waves show different transmission characteristics. For $f = 44.9$ GHz, the spin wave is bound to the modulator when it arrives, see $t = 1.0$ ns in Fig. 2(c), and spin waves propagate counterclockwise in the disk. While for $f = 49.1$ GHz, the spin wave can pass the modulator with almost no loss, see $t = 1.0$ ns in Fig. 2(d), and spin waves propagate clockwise in the disk. It is found that the transmission coefficient is related to the chirality of spin waves.

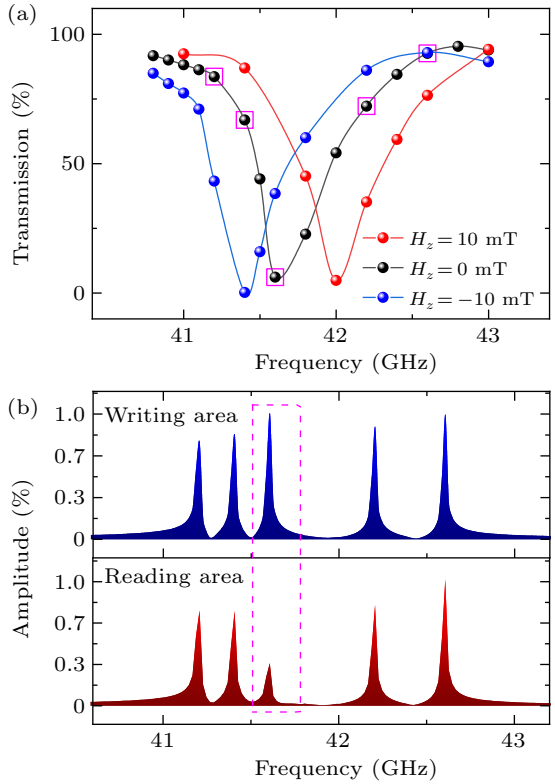


Fig. 3. (a) Frequency dependent transmissions of the band-stop filter under different magnetic fields H_z. (b) Intensity of spin waves with $f = 41.2$ GHz, 41.4 GHz, 41.6 GHz, 42.2 GHz, and 42.6 GHz for $H_z = 0$ mT in the writing area (top) and the reading area (bottom).

To further explore the working characteristics of the band-stop filter under different magnetic fields, we studied the transmission properties of spin waves in the frequency range from 41 GHz to 43 GHz. As shown in Fig. 3(a), the working frequency increases from 41.4 GHz to 42.0 GHz with its 3 dB bandwidth unchanged when external field H_z increases from -10 mT to 10 mT. The reason for this is that the increase of H_z causes the increase of the system energy, but does not change the magnetization of the band-stop filter. For $H_z = 0$ mT, the filter has an operating frequency of 41.6 GHz, transmission coefficient T of as low as 6%, and 3 dB bandwidth of around 0.5 GHz. Because its 3dB bandwidth is very narrow, it has a strong ability to block spin waves at specific frequencies. Hence, the proposed band-stop filter can effectively filter out spin waves at irrelevant interfering frequencies during the process of information transmission. Next, we demonstrated its filtering function by simultaneously inputting five frequencies, i.e., $f_1 = 41.2$ GHz, $f_2 = 41.4$ GHz, $f_3 = 41.6$ GHz, $f_4 = 42.2$ GHz, and $f_5 = 42.6$ GHz, as indicated by boxes in Fig. 3(a). These spin waves were excited by a perturbation field in the form $h_x(t) = h_0 \sum_{n=1}^{5} \sin(2\pi f_n t)$, where $h_0 = 10$ mT. The calculated spin wave intensities in the writing/reading areas are shown in the top/bottom panels of Fig. 3(b). It can be clearly found that the spin wave of the working frequency $f_3 = 41.6$ GHz is highly suppressed. However, spin waves of the non-working frequency are nearly not affected, for instance, $f_5 = 42.6$ GHz. It should be pointed out that the filtering function of the proposed band-stop filter can be extended from single frequency to multi-frequencies.

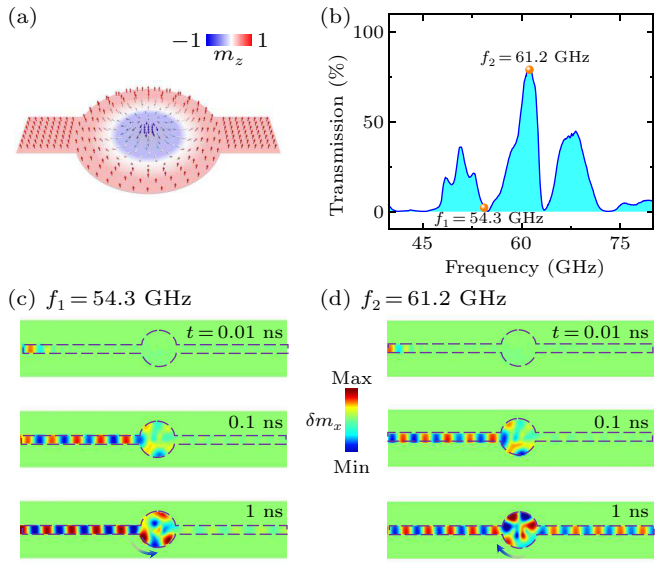


Fig. 4. (a) Magnetization of non-uniformly magnetized band-pass filter. (b) Calculated transmission dependence of spin waves on frequencies under zero field. Temporal snapshots of spin waves propagating in the filter at $t = 0.01$ ns, 0.1 ns, and 1 ns for (c) $f_1 = 54.3$ GHz and (d) $f_2 = 61.2$ GHz as marked in panel (b).

Secondly, we studied the transmission characteristics of spin waves in the band-pass filter shown in Fig. 1(a), in which the central part of the waveguide is designed as a circular modulator. The magnetization of the filter is perpendicularly magnetized with the presence of a Néel type skyrmion in the modulator as shown in Fig. 4(a). And the nucleated skyrmion can exist in the field range from -100 mT to 150 mT. The calculated transmission in the frequency range from 40 GHz to 80 GHz at $H_z = 0$ mT is shown in Fig. 4(b). It can be clearly found that the transmission of spin waves is different from that in Fig. 2(b). In Fig. 4(b), the transmission coefficients T of spin waves with most frequencies are below 20%, while those

of only a few frequencies are above 70%. Therefore, the device in Fig. 4(a) can be used as a band-pass filter. It should be pointed out that the introduction of the skyrmion ensures the performance of the band-pass filter. To demonstrate the function of the band-pass filter, we selected spin waves with frequencies 54.3 GHz and 61.2 GHz to display their propagation characteristics. The calculated temporal snapshots of spin waves propagating in the filter at $t = 0.01$ ns, 0.1 ns, and 1.0 ns are shown in Figs. 4(c) and 4(d). For $f = 54.3$ GHz, the spin wave is bound to the central modulator when it arrives, see $t = 1.0$ ns in Fig. 4(c), and spin waves propagate counterclockwise in the disk. While for $f = 61.2$ GHz, the spin wave can pass the modulator with negligible loss, see $t = 1.0$ ns in Fig. 4(d), and spin waves propagate clockwise in the disk.

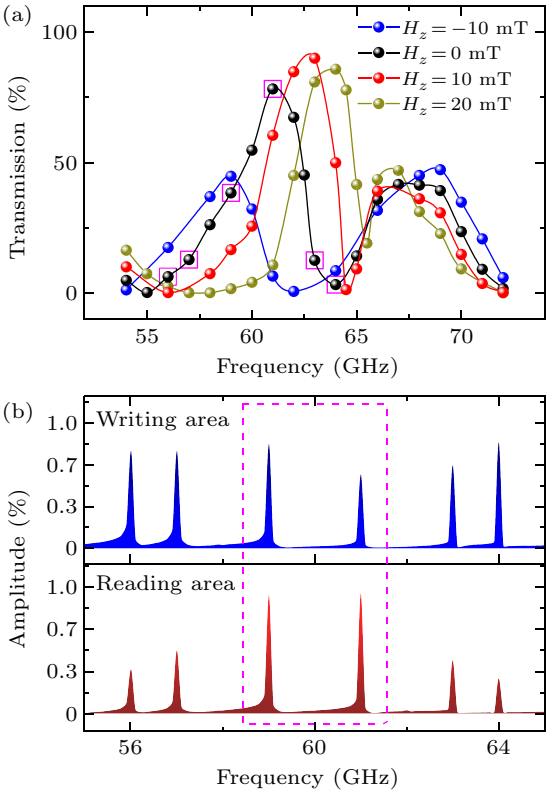


Fig. 5. (a) Frequency dependent transmissions of the band-stop filter under different magnetic fields H_z. (b) Intensity of spin waves with $f = 56$ GHz, 57 GHz, 59 GHz, 61 GHz, 63 GHz, and 64 GHz for $H_z = 0$ mT in the writing area (top) and the reading area (bottom).

Furthermore, the effect of magnetic field on the transmission properties of the band-pass filter in the frequency range from 54 GHz to 72 GHz was also studied as shown in Fig. 5(a). The working frequency increases from 59 GHz to 64 GHz, the transmission coefficient T increases from 45% to 90%, and the -3 dB bandwidth narrows when external field H_z increases from -10 mT to 20 mT. It should be noted that the diameter of the skyrmion is changed around 2 nm. For $H_z = 0$ mT, the working frequency of the filter is 61 GHz, and the maximum transmission is 78% with a -3 dB bandwidth of around 3.5 GHz. Finally, we verified its function by simultaneously inputting six frequencies by a perturbation field $h_x(t) = h_0 \sum_{n=1}^{6} \sin(2\pi f_n t)$ with $h_0 = 10$ mT, i.e., $f_1 = 56$ GHz, $f_2 = 57$ GHz, $f_3 = 59$ GHz, $f_4 = 61$ GHz, $f_5 = 63$ GHz, and $f_6 = 64$ GHz, as indicated by boxes in Fig. 5(a). The calculated spin wave intensities in the writing/reading areas are shown in the top/bottom panels of Fig. 5(b). It is obvious that the intensity attenuation of spin waves, whose working frequency is located in the operating bandwidth frequency range, is weak when they pass through the filter, for instance, $f_3 = 59$ GHz and $f_4 = 61$ GHz. However, for spin waves whose working frequencies are located out of the operating bandwidth frequency range, they are suppressed. It should be pointed out that the filtering function of the proposed band-pass filter can be extended from single frequency to multi-frequencies.

4. Conclusion and perspectives

In conclusion, we have numerically established the magnonic model of a band-pass filter and band-stop filter and verified the authenticity of their functional implementation. Depending on the magnetization in the modulator, the magnonic filter can work functionally as a band-pass or a band-stop. In addition, the operating frequency of the proposed filters can be changed by altering the external magnetic field, proving the possibility of reconfiguration of the device. It is found that the transmission-coefficient is related to the chirality of spin waves. And there are binding energies in the band-stop filter disk for spin waves with low transmission. These models can effectively filter the interference frequency and realize the effective transmission of information in the case of multiple inputting spin waves. Our findings could enrich the development of magnonic devices with spin textures.

Data availability statement

The data that support the findings of this study are openly available in Science Data Bank at the following link https://doi.org/10.57760/sciencedb.j00113.00051.

Acknowledgment

Project supported by the National Natural Science Foundation of China (Grant Nos. 12074189 and 11704191).

References

[1] Bohr M T and Young I A 2017 *IEEE Micro* **37** 20
[2] Track E, Forbes N and Strawn G 2017 *Comput. Sci. Eng.* **19** 4
[3] Guo P F, Yang L T, Yang Y, Fan L, Han G Q, Samudra G S and Yeo Y C 2009 *IEEE Electron Device Lett.* **30** 981
[4] Schwierz F 2010 *Nat. Nanotechnol.* **5** 487
[5] Manipatruni S, Nikonov D E and Young I A 2018 *Nat. Phys.* **14** 338
[6] Nikonov D E and Young I A 2013 *Proc. IEEE* **101** 2498
[7] Krivosik P and Patton C E 2010 *Phys. Rev. B* **82** 184428
[8] Kruglyak V V., Demokritov S O and Grundler D 2010 *J. Phys. D: Appl. Phys.* **43** 264001
[9] Chumak A V and Schultheiss H 2017 *J. Phys. D: Appl. Phys.* **50** 300201

[10] Kajiwara Y, Harii K, Takahashi S, Ohe J, Uchida K, Mizuguchi M, Umezawa H, Kawai H, Ando K, Takanashi K, Maekawa S and Saitoh E 2010 *Nature* **464** 262

[11] Kampfrath T, Sell A, Klatt G, Pashkin A, Mährlein S, Dekorsy T, Wolf M, Fiebig M, Leitenstorfer A and Huber R 2011 *Nat. Photonics* **5** 31

[12] Kostylev M P, Serga A A, Schneider T, Leven B and Hillebrands B 2005 *Appl. Phys. Lett.* **87** 153501

[13] Louis S, Lisenkov I, Nikitov S, Tyberkevych V and Slavin A 2016 *AIP Adv.* **6** 065103

[14] Vedmedenko E Y, Kawakami R K, Sheka D D, Gambardella P, Kirilyuk A, Hirohata A, Binek C, Chubykalo-Fesenko O, Sanvito S, Kirby B J, Grollier J, Everschor-Sitte K, Kampfrath T, You C Y and Berger A 2020 *J. Phys. D: Appl. Phys.* **53** 453001

[15] Chumak A V., Vasyuchka V I, Serga A A and Hillebrands B 2015 *Nat. Phys.* **11** 453

[16] Sheng L T, Chen J L and Yu H M 2021 *Mater. China* **40** 939

[17] Wang Q, Pirro P, Verba R, Slavin A, Hillebrands B and Chumak A V 2018 *Sci. Adv.* **4** e1701517

[18] Wang Q, Chumak A V and Pirro P 2021 *Nat. Commun.* **12** 2636

[19] Wang Q, Hamadeh A, Verba R, Lomakin V, Mohseni M, Hillebrands B, Chumak A V. and Pirro P 2020 *npj Comput. Mater.* **6** 192

[20] Chumak A V, Serga A A and Hillebrands B 2014 *Nat. Commun.* **5** 4700

[21] Schneider T, Serga A A, Leven B, Hillebrands B, Stamps R L and Kostylev M P 2008 *Appl. Phys. Lett.* **92** 022505

[22] Jamali M, Kwon J H, Seo S M, Lee K J and Yang H 2013 *Sci. Rep.* **3** 3160

[23] Au Y, Dvornik M, Dmytriiev O and Kruglyak V V 2012 *Appl. Phys. Lett.* **100** 172408

[24] Wang Q, Kewenig M, Schneider M, Verba R, Kohl F, Heinz B, Geilen M, Mohseni M, Lägel B, Ciubotaru F, Adelmann C, Dubs C, Cotofana S D, Dobrovolskiy O V, Brächer T, Pirro P and Chumak A V 2020 *Nat. Electron.* **3** 765

[25] Talmelli G, Devolder T, Träger N, Förster J, Wintz S, Weigand M, Stoll H, Heyns M, Schütz G, Radu I P, Gräfe J, Ciubotaru F and Adelmann C 2020 *Sci. Adv.* **6** eabb4042

[26] Fischer T, Kewenig M, Bozhko D A, Serga A A, Syvorotka I I, Ciubotaru F, Adelmann C, Hillebrands B and Chumak A V 2017 *Appl. Phys. Lett.* **110** 152401

[27] Nikitin A A, Ustinov A B, Semenov A A, Chumak A V, Serga A A, Vasyuchka V I, Lähderanta E, Kalinikos B A and Hillebrands B 2015 *Appl. Phys. Lett.* **106** 102405

[28] Chen X X, Wang Q, Zhang H W and Zhong Z Y 2015 *Micronanoelectronic Technology* **52** 485

[29] Zhang Z K, Jin L C, Wen T L, Liao Y L, Tang X L, Zhang H W and Zhong Z Y 2020 *Sci. Sin. Informationis* **50** 67

[30] Heussner F, Talmelli G, Geilen M, Heinz B, Brächer T, Meyer T, Ciubotaru F, Adelmann C, Yamamoto K, Serga A A, Hillebrands B and Pirro P 2020 *Phys. Status Solidi - Rapid Res. Lett.* **14** 1900695

[31] Torrejon J, Riou M, Araujo F A, Tsunegi S, Khalsa G, Querlioz D, Bortolotti P, Cros V, Yakushiji K, Fukushima A, Kubota H, Yuasa S, Stiles M D and Grollier J 2017 *Nature* **547** 428

[32] Brächer T and Pirro P 2018 *J. Appl. Phys.* **124** 152119

[33] Belmeguenai M, Adam J P, Roussigné Y, Eimer S, Devolder T, Kim J Von, Cherif S M, Stashkevich A and Thiaville A 2015 *Phys. Rev. B* **91** 180405

[34] Di K, Zhang V L, Lim H S, Ng S C, Kuok M H, Qiu X and Yang H 2015 *Appl. Phys. Lett.* **106** 052403

[35] Bisero D 2020 *Magnetochemistry* **6** 40

[36] Jibiki Y, Goto M, Tamura E, Cho J, Miki S, Ishikawa R, Nomura H, Srivastava T, Lim W, Auffret S, Baraduc C, Bea H and Suzuki Y 2020 *Appl. Phys. Lett.* **177** 082402

[37] Vansteenkiste A and De Wiele B Van 2011 *J. Magn. Magn. Mater.* **323** 2585

[38] Di K, Zhang V L, Lim H S, Ng S C, Kuok M H, Qiu X and Yang H 2015 *Appl. Phys. Lett.* **106** 052403

[39] Zhang V L, Hou C G, Di K, Lim H S, Ng S C, Pollard S D, Yang H and Kuok M H 2017 *AIP Adv.* **7** 055212

[40] Ma F S, Lim H S, Wang Z K, Piramanayagam S N, Ng S C and Kuok M H 2011 *Appl. Phys. Lett.* **98** 153107